





Article

Correlation between LAA Morphological Features and Computational Fluid Dynamics Analysis for Non-Valvular Atrial Fibrillation Patients

Benigno Marco Fanni ^{1,2,†,‡} , Katia Capellini ^{1,2,‡}, Mario Di Leonardo ¹, Alberto Clemente ³ , Elisa Cerone ⁴, Sergio Berti ⁴  and Simona Celi ^{1,*,†} 

¹ BioCardioLab, Fondazione Toscana Gabriele Monasterio, Via Aurelia Sud, 54100 Massa, Italy; bmfanni@ftgm.it (B.M.F.); kcapellini@ftgm.it (K.C.); mariodileon@gmail.com (M.D.L.)

² Department of Information Engineering, University of Pisa, Via Girolamo Caruso 16, 56122 Pisa, Italy

³ Radiology Unit, Fondazione Toscana Gabriele Monasterio, Via Aurelia Sud, 54100 Massa, Italy; alberto.clemente@ftgm.it

⁴ Adult Cardiology Unit, Fondazione Toscana Gabriele Monasterio, Via Aurelia Sud, 54100 Massa, Italy; elisa.cerone@libero.it (E.C.); berti@ftgm.it (S.B.)

* Correspondence: s.celi@ftgm.it; Tel.: +39-0585-493682

† Current address: Via Aurelia Sud, Heart Hospital, 54100 Massa, Italy.

‡ These authors contributed equally to this work.

Received: 29 January 2020; Accepted: 18 February 2020; Published: 20 February 2020



Abstract: The left atrial appendage (LAA) is a complex cardiovascular structure which can yield to thrombi formation in patients with non-valvular atrial fibrillation (AF). The study of LAA fluid dynamics together with morphological features should be investigated in order to evaluate the possible connection of geometrical and hemodynamics indices with the stroke risk. To reach this goal, we conducted a morphological analysis of four different LAA shapes considering their variation during the cardiac cycle and computational fluid dynamics (CFD) simulations in AF conditions were carried out. The analysis of main geometrical LAA parameters showed a huger ostium and a reduced motility for the cauliflower and cactus shapes, as well as a lower velocity values from the CFD analysis. Such findings are in line with literature and highlight the importance of coupling dynamics imaging data with CFD calculations for providing information not available at clinical level.

Keywords: left atrial appendage; atrial fibrillation; computational fluid dynamics; image processing; morphological analysis

1. Introduction

Atrial fibrillation (AF) is a condition affecting the normal sinus rhythm of the heart and it is strongly related to the risk of strokes [1]. In this context, it was proven that the hemodynamics of the left atrium (LA) and in particular the fluid dynamics characteristics of the left atrial appendage (LAA) play an important role in the stroke risk determination [2]. In fact, especially in non-valvular AF patients with contraindication to anticoagulation therapy, LAA is responsible for the formation of more than 90% of thrombi which can yield to cardioembolic events [3]. Presently, LAA occlusion is a diffused treatment strategy to reduce the migration of thrombi and the associated cardioembolic risk [4,5]. This procedure is particularly challenging due to the LAA morphological and hemodynamics complexity [6].

The morphology of the LAA is quite variable and it is commonly classified into four main shape classes: “chicken wing” (CW) (48%), “cactus” (CS) (30%), “windsock” (WS) (19%), and “cauliflower” (CF) (3%) [7]. In non-valvular AF conditions, the normal contractility of LAA is reduced, resulting in a high decreasing of velocity and, consequently, in a higher risk of clotting formation due to the

hemostasis of the blood inside the LAA. Computational fluid dynamics (CFD) is turning out to be a useful instrument to evaluate LAA hemodynamic indicators such as velocity patterns, vorticity, wall shear stress and pressure [8–10]. The impact of AF on different LAA shapes hemodynamics was recently investigated in [11] highlighting the influence of LAA morphology on the blood velocity patterns although a quantitative assessment and correlation with geometrical features for the different shapes is missing. The changes in LAA position and morphology during cardiac cycle due to the LA motion are significant aspects to be considered in the LAA geometric evaluation [12]. Even if there are few studies in the literature that analyze LAA geometrical features [13,14], to the best of our knowledge the variation of relevant LAA geometrical parameters have not been yet investigated. Hence, it is crucial to develop methods able to identify a correlation between morphological and flow dynamics parameters to prevent thrombi formation.

This study aims to evaluate the dynamic of LAA geometrical indicators during cardiac cycle and the related hemodynamics by developing a computational model able to perform an accurate LA and LAA fluid dynamic analysis in order to investigate the correlation between LAA different shapes and stroke risk.

2. Material and Methods

In this work the investigation of the LAA morphology and hemodynamics was conducted both considering computer simulations and medical images analysis. An in-silico approach was adopted to assess the fluid dynamics within the LAA for each main shape group in pathological conditions. In addition, image analysis was conducted to verify the correlation between LAA morphological parameters and fluid dynamics indexes. Despite the complex geometry of the LAA, in the present study, the classification of LAA morphologies reported by Kimura et al. [15] was adopted.

2.1. Image Acquisition

ECG-gated computed tomography (CT) images from four patients who underwent LAA occlusion were considered in this study. Each acquisition comprised 10 phases of the cardiac cycle (from 0% to 90%), for a total of 40 volumetric dataset. Patients were selected as clinical cases of relevant interest from specialist doctors to cover the four different LAA shape groups (CW, CF, WS and CS). CT images were acquired with a 320-detector scanner (Toshiba Aquilion One, Toshiba, Japan), using contrast medium. Images were characterized by a dimension of 512×512 pixels with a bit depth of 16 and a spatial resolution of 0.495 mm^3 .

2.2. Image and Morphological Analysis

For each dataset, all the phases of the cardiac cycle were segmented in the open source software Slicer (www.slicer.org) [16] using a thresholding technique in order to obtain the 3D LAA geometries (Figure 1a–d). Final patient-specific models consisted of the LA with respective LAA, the pulmonary veins (PVs) and the mitral valve (MV) orifice.

Finally, each dataset was analysed with a specific VMTK-Python script in order to extract morphological parameters of the LAA along the cardiac cycle, i.e., the LAA volume, the surface of the ostium (A_o) (Figure 1e), the LAA centerline length $C(s)$ and tortuosity [17]. In this work the centerline calculation is traced from the points P_o and P_t , where P_o is the centroid of the surface of the ostium and P_t is the tip of the LAA. To ensure that the final $C(s)$ is central, its paths (s) is bound to run on the Voronoi diagram of the model. In the case of more relevant tips in same LAA shape the longer centerline was considered. For the calculation of the tortuosity Equation (1) was adopted:

$$T = \frac{C(s)}{P_o P_t} - 1 \quad (1)$$

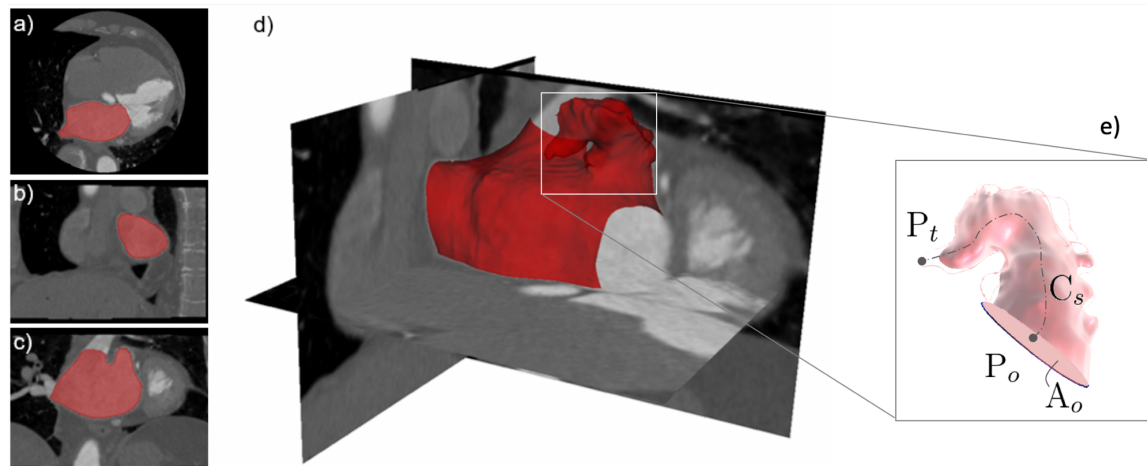


Figure 1. Example of volumetric CT segmentation with axial (a), sagittal (b) and coronal (c) planes and resulted 3D model (d). Identification of the area of the ostium (A_o) and of the centerline $C(s)$ from P_o , where P_t (e).

2.3. Numerical Simulations

CFD analysis of the four patient-specific cases were carried out in a dynamic regime. ANSYS Fluent (ANSYS Inc, Canonsburg, USA) was used to solve the Navier-Stokes governing equations of the fluid. The CT images belonging to the mid-diastolic phase of the cardiac cycle (equivalent to 60%) were used to build the numerical models of the four cases.

Following sensitivity mesh-analysis, a volumetric grid with tetrahedral and hexahedral elements was generated for all the models. Final meshes counted 2,362,103 elements for the chicken wing model, 3,964,963 for the cauliflower model, 1,932,011 for the windsock model and 4,218,847 for cactus model. Hexahedral elements were used along the wall of the models, where a 5-layers inflation was generated.

To take into account for the opening and closure actions of the valve during the cardiac cycle, a transient velocity outflow condition was assigned to the MV orifices. Following this strategy, the closure period of the MV, i.e., the ventricular systole, was simulated when a null velocity occurred, while the non-zero velocity values corresponded to the passage of the blood flow during the ventricular diastole, i.e., when the valve is open. A velocity profile representative of the atrial fibrillation (AF) condition was imposed at the MV section [18], while a transient pressure profile was assigned at the PVs (Figure 2). The pressure profile was generated based on a custom script taking into account for the MV velocity and the physiological pressure range of the LA (5–13 mmHg) during the cardiac cycle. The wall was assumed as rigid with no-slip condition.

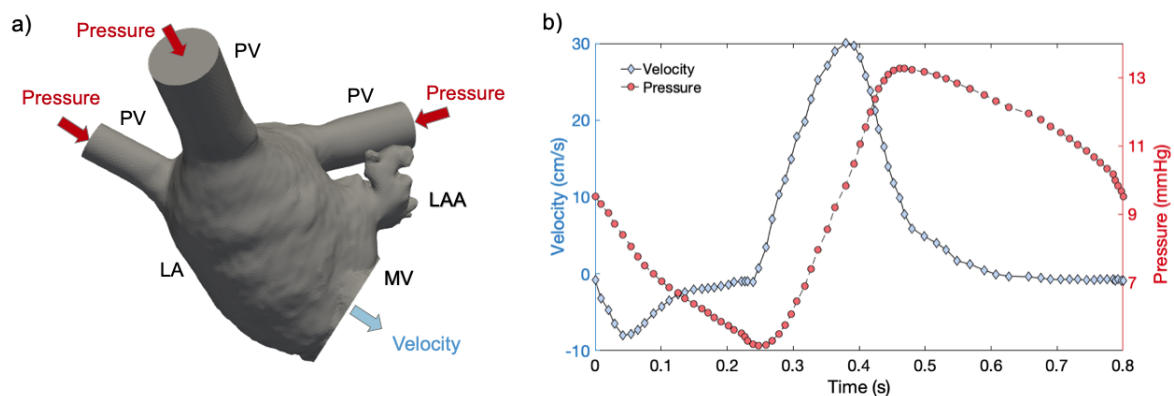


Figure 2. CFD model of LA with LAA, PVs and MV, including inflow pressure boundaries (marked in red) and velocity outflow boundary (marked in blue) (a). PVs inflow pressure and MV outflow velocity curves during cardiac cycle (b).

The blood was treated as Newtonian and incompressible, as widely accepted to model blood in cardiovascular problems [8–11,14,19,20] with a density of 1060 kg/m^3 and a viscosity of 0.0035 Pa s . A laminar model was implemented based on the calculation of the Reynolds number [11].

All the simulations were run for four cardiac cycles, with each cardiac cycle lasting 0.8 s , to allow the full development of the flow. The time domain was discretized with a time step of 0.005 s . The hemodynamics analysis was performed in the last cycle to avoid the inclusion of nonlinear start-up effects.

CFD simulations were evaluated in terms of velocity fields. Velocity and pressure patterns were visually analysed to assess the correct implementation of the atrial flow direction. In particular, velocity fields were analyzed in the LAA portion of the four cases. Three planes of analysis were created, corresponding to the ostium plane, a middle plane and a distal plane, and the mean through-plane velocity was computed.

3. Results

3.1. Image and Morphological Analysis

The resulted 3D models of the four representative cases are shown in Figure 3. According to the international classification, LAAs are classified into the following four types: (i) “chicken wing”, a $>4\text{-cm}$ -long main lobe with a folded angle of $<100^\circ$ (Figure 3a); (ii) “cauliflower”, a $<4\text{-cm}$ -long main lobe with no forked lobes (Figure 3b); (iii) “windsock”, a main lobe $>4 \text{ cm}$ long with a folded angle of $>100^\circ$ (Figure 3c); (iv) “cactus”, a $<4\text{-cm}$ -long main lobe with more than two lobes over 1 cm (Figure 3d).

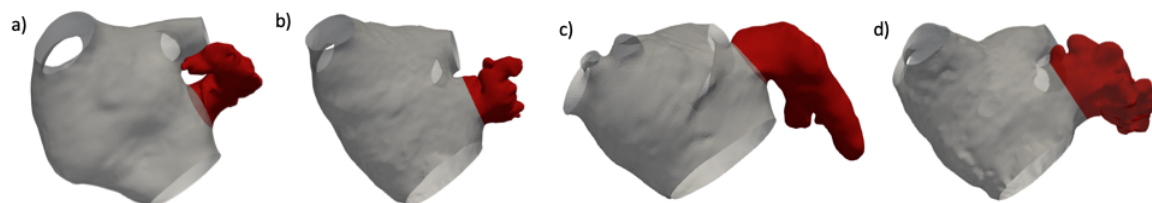


Figure 3. Example of 3D models for each LAA morphologies: Chicken wing (a), Cauliflower (b), Windsock (c) and Cactus (d).

For all the patients, the reconstruction of all the cardiac phases was feasible. Figure 4 shows the geometrical variation of the LAA models along the heartbeat.

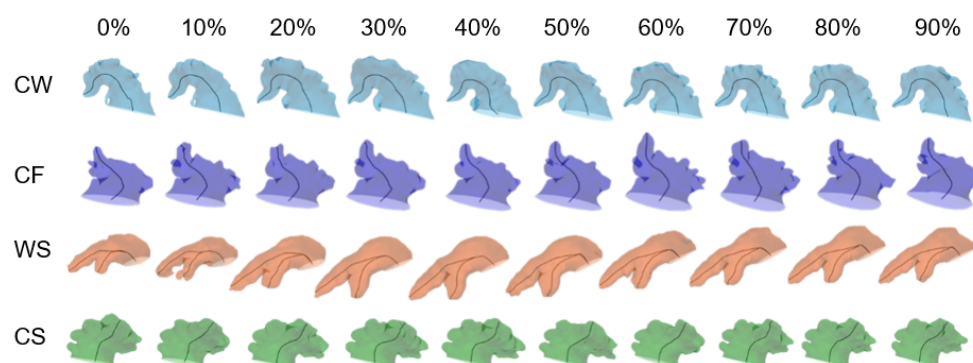


Figure 4. Shape variation over the ten phases of the cardiac cycle for all the LAA morphologies.

The calculated morphological indexes along the cardiac cycle are reported in Figure 5 for all the four morphologies, in terms of boxplots.

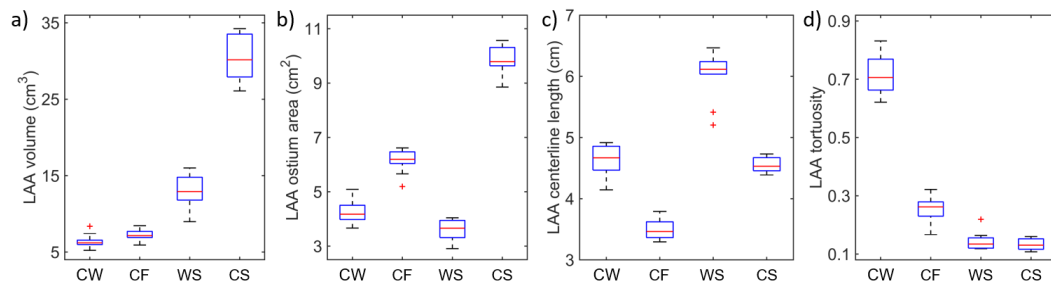


Figure 5. Boxplots of volume (a), ostium area (b), centerline length (c) and tortuosity (d) measurements of LAA morphologies over a cardiac cycle.

3.2. CFD Analysis

CFD models were successfully implemented and all the solutions reached convergence. Velocity patterns were analyzed to qualitatively and quantitatively assess the perfusion of the LAAs along the cardiac cycle. Figure 6 shows the velocity streamlines for all the models in two selected time instants, i.e., at velocity peak (t_1 , when the valve is open) and at the end of the cardiac cycle (t_2 , when the valve is closed and the fluid is circulating within the LA). Details of the velocity fields for all the four LAA shapes are showed in Figure 7, in which three particular time instants are depicted, i.e., before the velocity peak (t_0), at the velocity peak (t_1) and after (t_2). Volume cells with a velocity values below 0.001 cm/s were highlighted in Figure 8, reporting also the percentage volume with extremely low velocity for each LAA shape. A quantitative analysis of the velocity trend along the LAA, from the ostium of the distal tip, was performed (Figure 9).

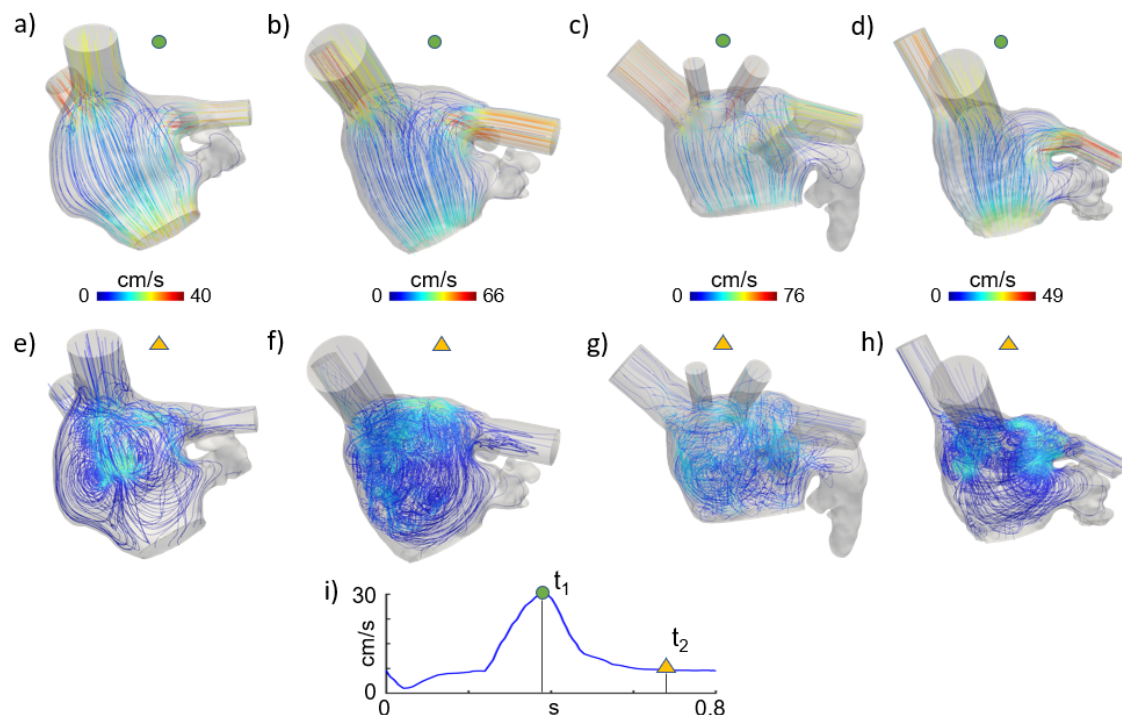


Figure 6. Velocity streamlines of each LAA morphology, i.e., CW (a,e), CF (b,f), WS (c,g) and CS (d,h) with the respective LA at t_1 time (a–d) and at t_2 time (e–h) of the cardiac cycle in terms of MV velocity profile (i).

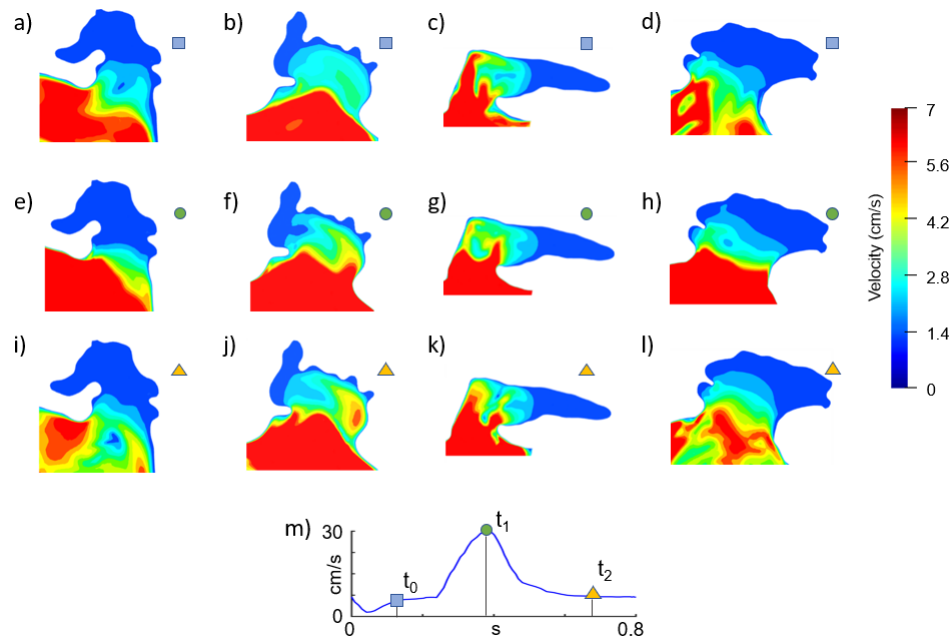


Figure 7. Velocity fields of the four LAA shapes, i.e., CW (a,e,i), CF (b,f,j), WS (c,g,k) and CS (d,h,l) at t_0 time (a–d), t_1 time (e–h) and t_2 time (i–l) of the cardiac cycle in terms of MV velocity profile (m).

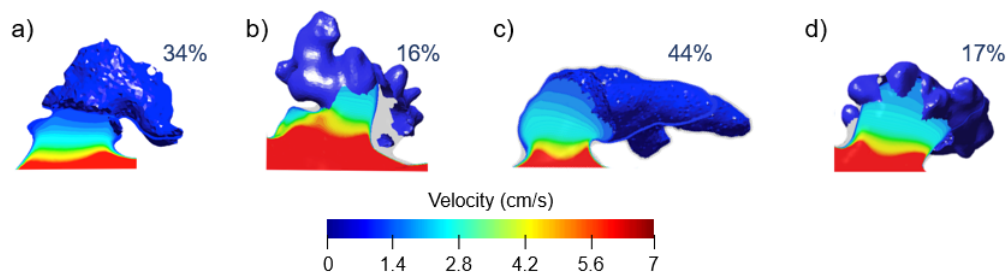


Figure 8. Velocity field for a specific plane with overlapped volume cells presenting a velocity value below 0.001 cm/s for CW (a), CF (b), WS (c) and CS shape (d).

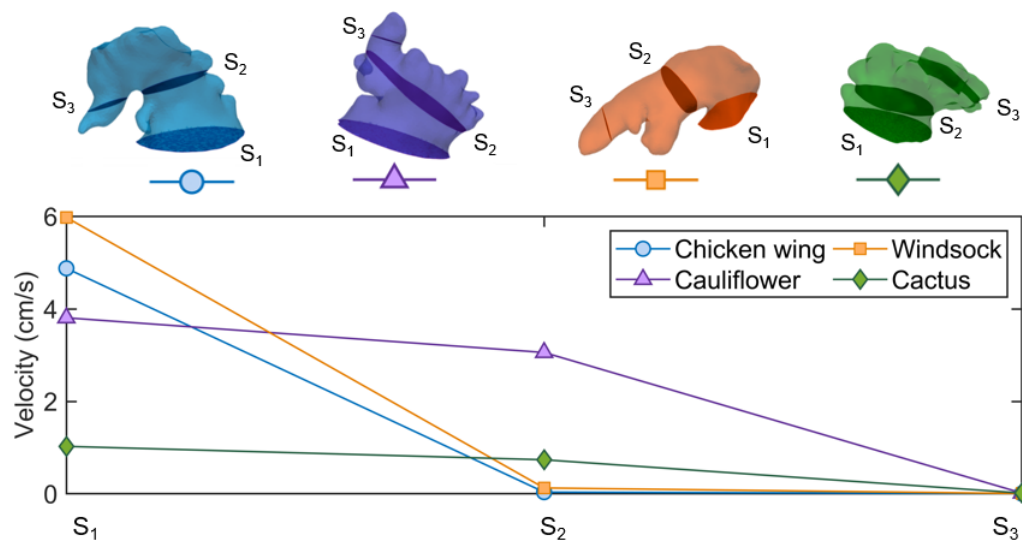


Figure 9. Flow velocity at three different planes: ostium section (S_1), mid section (S_2) and distal tip section (S_3).

4. Discussion

In this study, we assessed the influence of the LAA morphology and hemodynamics on the stroke risk in patients affected by non-valvular AF condition. Regarding the morphological features, currently, there is a strong necessity to understand the anatomical properties of the LAA during the cardiac cycle. This effort arises from a twofold need: from one side, to stratify the risk of LAA thrombus formation in AF patients, and, on the other hand, to develop new percutaneous closure procedures. Previous studies have demonstrated the alterations in shape, size and contraction patterns of LAA in AF condition by using different imaging techniques [12,21–23].

In the work presented here, the LAA morphological parameters were analysed along the entire cardiac cycle by using ECG-gated CT images, as several studies have assessed the correlation between image-based variables with increased risk of stroke in AF patients [24–26]. The processing of CT images in all the phases of the cardiac cycle allowed to highlight the main differences between patients in terms of motility of the respective LAA. Figure 4 allows qualitatively notifying the changes of all the LAAs along the cardiac cycle. The quantitative analysis of the LAA volume, ostium area, centerline length and tortuosity is shown in Figure 5, where it is possible to verify the considerable variability of the analyzed morphological parameters among different LAAs and within the cardiac cycle. Starting from the LAA volume analysis (Figure 5a), the CS shape resulted in being the biggest and with more variability, while the CW and the CF morphologies were small and characterised by low expansions during the cardiac cycle. For the ostium area quantification (Figure 5b), the trend was different and CF and CS cases showed a huger ostium than CW and WS shapes. This result may suggest that CF and CS morphologies presented low flow velocities, as a big ostium is usually related to blood stagnation and thus a higher risk of thrombi formation [27,28]. On the other hand, the analysis of centerline variation (Figure 5c) along the cardiac cycle confirmed such scenario, where CF and CS shapes presented a low length as well as a low variability suggesting a reduced LAA motility. Finally, the tortuosity analysis (Figure 5d) showed that the CW morphology presented the highest value and the highest variability, which reflect the high curvature of the shape as appreciable in Figure 4. Centerline length and tortuosity trends of the LAAs for all the ten phases of the cardiac cycle (0–90%) are depicted in Figure 10, where values were calculated as percentage variation in respect to the 30% phase, i.e., when the atrial systole occurs. As we can see, the CF and CS shapes are characterised by a high value of tortuosity variation (about 30%) associated with a low centerline length variation (<10%). According to Equation (1), the combined effect of these two parameters produce a bending phenomenon, potentially suggesting an augmented risk of thrombus dislodgement and migration. The WS shape presented instead a slightly higher centerline and tortuosity values (Figure 10c) than the more critical CF and CS morphologies. This combined behaviour reduces the bending effect and potentially the risk of thrombus dislodgement. The CW shape resulted in being the less risky as centerline length variation were higher (Figure 10a), indicating a constant washout of the LAA during the cardiac cycle. The tortuosity variation for this model maintains a low value (<20%).

The CFD analysis showed similar global velocity fields for the four studied cases (Figure 6). Locally, very low velocities were found in the LAAs in respect to the global scale (Figure 7). This trend is in line with previous CFD studies [11,14]. Considerations of specific planes for each LAA (Figure 9a) allowed a shape-specific velocity analysis showing how differently the blood flow decreases from the ostium to the tip (Figure 9b). In particular, while CW and WS shapes showed relatively high velocities at ostium level, rapidly decreasing in the middle planes, CF and CS morphologies were characterized by an overall low velocity, especially for the CS case. Such condition may indicate a higher probability of blood stagnation and thus a major probability of thrombi formation. Furthermore, the CF and CS analyzed shapes present a high number of lobes (10 and 9 respectively) in respect to CW and WS (5 and 3). Recent study has demonstrated that there is a significant correlation between the number of lobes and the risk of thromboembolic events [29]. Reasonably, the formation of a small thrombus is higher than a big one. In this vein, in Figure 7, the volume representing the cells with extremely low velocity (<0.001 cm/s) was found to be higher in the cases of CW (Figure 8a) and WS (Figure 8c) in

respect to CF (Figure 8b) and CS (Figure 8d). Nevertheless, the volumes of CF and CS shapes appeared as composed of several small sub-volumes located in the lobes (Figure 8b–d).

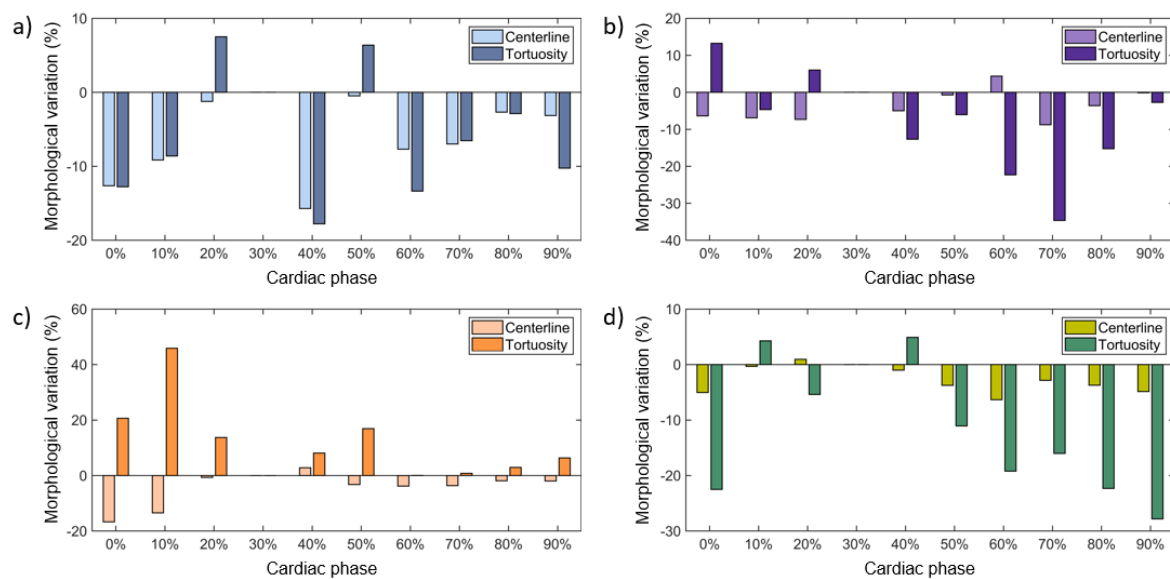


Figure 10. Variation of centerline and tortuosity indices at each phase of cardiac cycle for CW (a), CF (b), WS (c) and CS (d) shapes with respect to the systolic phase (30%).

The few CFD studies available on this topic [13,14] focused on the correlation between the flow simulation and the LAA morphologies only at a single instant of the cardiac cycle. Most of previous segmentation approaches were based on 3D rotational angiography [13,30] or standard CT technique [14], thus focusing on a static model for their morphological analysis. With respect to the previous works, we analyzed all the phases of the cardiac cycle.

The main finding of this work is that analysis of morphological and CFD results are consistent, since both image-based and computational strategies focus the attention on the CF and CS LAA shapes for stroke risk. On one hand, imaging elaboration highlighted a bigger ostium, which was already identified in the literature as a high risk factor for AF patients [31]. Moreover, a reduced motility for the CF and CS shapes in respect of CW and WS cases was found, as well as a higher number of lobes which may be representative of suitable sites for thrombi generation. On the other hand, CFD post-processing showed for CF and CS shapes relatively very low velocities in proximity of lobes, again supporting that these two morphologies could be more prone to develop thromboembolic events, as in accordance with clinical reports [24].

Our approach can be further improved. Obviously the clinical problem we are facing is very complex, as an interchangeable conditioning effect between the LA and the LAA shapes and both effects can be hypothesized and should be considered. Moreover, future developments will be focused on considering a larger number of patient-specific LAAs in order to fully investigate its wide anatomical variability and increase the statistical relevance of the study.

However, the investigation on the correlation between ECG-gated CT volumetric datasets along the cardiac cycle and CFD analyses is novel, as similar studies only considered single-phase CT datasets. However, the assumption of rigid wall in the numerical simulations could be strong, especially when it was verified from imaging analysis that the motility of the LAAs is not negligible. More complex strategies will be adopted to overcome such limitations, in order to take into account for the wall movements.

5. Conclusions

In this work, image elaboration and computational tools were used to assess the risk of thrombi generation in patients affected by non-valvular AF condition. Four cases representative of the main LAA shape groups were selected and investigated. The novelty of the study resides in the dynamical analysis of CT images along the cardiac cycle, which provided additional information to be coupled to computational analysis for the understanding of clots and thrombi generation. Both strategies indicated CF and CS shapes as being the more risky to generate clots, in accordance with literature. The workflow presented here should be further enhanced to assess more deeply the LAA hemodynamics and the related stroke risk, in order to prevent thromboembolic events and potentially increase the effectiveness of percutaneous interventions.

Author Contributions: Conceptualization, S.B. and S.C.; Data curation, B.M.F., K.C., A.C., E.C., S.B. and S.C.; Formal analysis, B.M.F., K.C. and M.D.L.; Investigation, B.M.F., K.C., E.C. and S.C.; Methodology, S.C.; Project administration, S.C.; Resources, S.B. and S.C.; Software, B.M.F., K.C. and M.D.L.; Supervision, S.C.; Validation, A.C., E.C. and S.B.; Visualization, B.M.F., K.C. and S.C.; Writing—original draft, B.M.F., K.C. and S.C.; Writing—review & editing, B.M.F., K.C. and S.C. Please turn to the <http://img.mdpi.org/data/contributor-role-instruction.pdf> for the term explanation. All authors have read and agreed to the published version of the manuscript.

Funding: This research received no external funding.

Conflicts of Interest: The authors declare no conflict of interest.

Abbreviations

The following abbreviations are used in this manuscript:

AF	Atrial Fibrillation
LA	Left Atrium
LAA	Left Atrium Appendage
CW	Chicken Wing
CS	Cactus
WS	Windsock
CF	Cauliflower
CFD	Computational Fluid Dynamics
CT	Computerised Tomography
PV	Pulmonary Vein
MV	Mitral Valve

References

1. Wolf, P.A.; Abbott, R.D.; Kannel, W.B. Atrial fibrillation as an independent risk factor for stroke: The framingham study. *Stroke* **1991**, *22*, 983–988. [\[CrossRef\]](#)
2. Gupta, D.K.; Shah, A.M.; Giugliano, R.P.; Ruff, C.T.; Antman, E.M.; Grip, L.T.; Mercuri, M. Left atrial structure and function in atrial fibrillation: Engage aftimi 48. *Eur. Heart J.* **2014**, *22*, 983–988. [\[CrossRef\]](#) [\[PubMed\]](#)
3. Holmes, D.R.; Lakkireddy, D.R.; Whitlock, R.P.; Waksman, R.; Mack, M.J. Left atrial appendage occlusion: opportunities and challenges. *J. Am. Coll. Cardiol.* **2014**, *63*, 291–298. [\[CrossRef\]](#) [\[PubMed\]](#)
4. Chanda, A.; Reilly, J.P. Left atrial appendage occlusion for stroke prevention. *Prog. Cardiovasc. Dis.* **2017**, *59*, 626–635. [\[CrossRef\]](#) [\[PubMed\]](#)
5. Berti, S.; Pastormerlo, L.E.; Celi, S.; Ravani, M.; Trianni, G.; Cerone, E.; Santoro, G. First-in-human percutaneous left atrial appendage occlusion procedure guided by real-time 3-dimensional intracardiac echocardiography. *JACC Cardiovasc. Interv.* **2018**, *11*, 2228–2231. [\[CrossRef\]](#) [\[PubMed\]](#)
6. Berti, S.; Pastormerlo, L.E.; Rezzaghi, M.; Trianni, G.; Paradossi, U.; Cerone, E.; Palmieri, C. Left atrial appendage occlusion in high-risk patients with non-valvular atrial fibrillation. *Heart* **2016**, *7*, 1036–1044. [\[CrossRef\]](#) [\[PubMed\]](#)
7. Beigel, R.; Wunderlich, N.C.; Ho, S.Y.; Arsanjani, R.; Siegel, R.J. The left atrial appendage: anatomy, function, and noninvasive evaluation. *JACC Cardiovasc. Imag.* **2014**, *7*, 1251–1265. [\[CrossRef\]](#)

8. Koizumi, R.; Funamoto, K.; Hayase, T.; Kanke, Y.; Shibata, M.; Shiraishi, Y.; Yambe, T. Numerical analysis of hemodynamic changes in the left atrium due to atrial fibrillation. *J. Biomech.* **2015**, *48*, 472–478. [[CrossRef](#)]
9. Otani, T.; Aa-Issa, A.; Pourmorteza, A.; McVeigh, E.R.; Wada, S.; Ashikaga, H. A Computational Framework for Personalized Blood Flow Analysis in the Human Left Atrium. *Ann. Biomed. Eng.* **2016**, *44*, 3284–3294. [[CrossRef](#)]
10. Masci, A.; Alessi, M.; Dedè, L.; Forti, D.; Menghini, F.; Tornasi, C.; Corsi, C. Development of a Computational Fluid Dynamics Model of the Left Atrium in Atrial Fibrillation on a Patient Specific Basis. *Comput. Cardiol.* **2017**. [[CrossRef](#)]
11. Bosi, G.M.; Cook, A.; Rai, R.; Menezes, L.J.; Schievano, S.; Torii, R.; Burriesci, G.B. Computational Fluid Dynamic Analysis of the Left Atrial Appendage to Predict Thrombosis Risk. *Front. Cardiovasc. Med.* **2018**, *4*, 34. [[CrossRef](#)] [[PubMed](#)]
12. Vivoli, G.; Gasparotti, E.; Rezzaghi, M.; Cerone, E.; Mariani, M.; Lini, L.; Celi, S. Simultaneous Functional and Morphological Assessment of Left Atrial Appendage by 3D Virtual Models. *J. Healthc. Eng.* **2019**, *7*, 1–8. [[CrossRef](#)] [[PubMed](#)]
13. García Isla, G.; Olivares, A.L.; Silva, E.; Nuñez-García, M.; Butakoff, C.; Sanchez-Quintana, D.; Camara, O. Sensitivity analysis of geometrical parameters to study haemodynamics and thrombus formation in the left atrial appendage: Virtual Haemodynamics and thrombus formation study in LAA. *Int. J. Numer. Method Biomed. Eng.* **2018**, *8*, e3100. [[CrossRef](#)] [[PubMed](#)]
14. Masci, A.; Barone, L.; Dedè, L.; Fedele, M.; Tomasi, C.; Quarteroni, A.; Corsi, C. The Impact of Left Atrium Appendage Morphology on Stroke Risk Assessment in Atrial Fibrillation: A Computational Fluid Dynamics Study. *Front. Physiol.* **2018**, *22*, 1938. [[CrossRef](#)] [[PubMed](#)]
15. Kimura, T.; Takatsuki, S.; Inagawa, K.; Katsumata, Y.; Nishiyama, T.; Nishiyama, N.; Jinzaki, M. Anatomical characteristics of the left atrial appendage in cardiogenic stroke with low CHADS2 scores. *Heart Rhythm* **2013**, *10*, 921–925. [[CrossRef](#)]
16. Kikinis, R.; Pieper, S.D.; Vosburgh, K. *3D Slicer: A Platform for Subject-Specific Image Analysis, Visualization, and Clinical Support. Intraoperative Imaging and Image-Guided Therapy*; Springer: New York, NY, USA, 2014; pp. 277–289.
17. Antiga, L.; Steinman, D.A. Robust and objective decomposition and mapping of bifurcating vessels. *IEEE Trans. Med. Imag.* **2004**, *23*, 704–714. [[CrossRef](#)]
18. International Organization for Standardization. *ISO 4850-1:2015 Cardiovascular Implants—Cardiac Valve Prostheses Part 1: General Requirements*; International Organization for Standardization: Geneva, Switzerland, 2015; p. 4850.
19. Boccadifuoco, A.; Mariotti, A.; Capellini, K.; Celi, S.; Salvetti, M.V. Validation of Numerical Simulations of Thoracic Aorta Hemodynamics: Comparison with In Vivo Measurements and Stochastic Sensitivity Analysis. *Cardiovasc. Eng. Technol.* **2018**, *9*, 688–706.
20. Capellini, K.; Vignali, E.; Costa, E.; Gasparotti, E.; Biancolini, M.E.; Lini, L.; Celi, S. Computational fluid dynamic study for aTAA hemodynamics: an integrated image-based and RBF mesh morphing approach. *J. Biomech. Eng.* **2018**. [[CrossRef](#)]
21. Chen, R.; Wu, X.; Jin, H.; Wang, B.; Ma, M.; Zhao, B. Assessment of left atrial appendage morphology and function in patients with non-valvular paroxysmal atrial fibrillation with different rhythms using real-time 3D transesophageal echocardiography. *Ultrasound Med. Biol.* **2016**, *42*, 118–124. [[CrossRef](#)]
22. Matsumoto, Y.; Morino, Y.; Kumagai, A.; Hozawa, M.; Nakamura, M.; Terayama, Y.; Tashiro, A. Characteristics of anatomy and function of the left atrial appendage and their relationships in patients with cardioembolic stroke: a 3-dimensional transesophageal echocardiography study. *J. Stroke Cerebrovasc. Diag.* **2017**, *26*, 470–479. [[CrossRef](#)]
23. Singh, S.M.; Jimenez-Juan, L.; Danon, A.; Bastarrika, G.; Shmatukha, A.V.; Wright, G.A.; Crystal, E. Magnetic resonance imaging of the left atrial appendage post pulmonary vein isolation: implications for percutaneous left atrial appendage occlusion. *J. Arrhythmia* **2015**, *31*, 108–113. [[CrossRef](#)]
24. Di Biase, L.; Santangeli, P.; Anselmino, M.; Mohanty, P.; Salvetti, I.; Gili, S.; Pump, A. Does the left atrial appendage morphology correlate with the risk of stroke in patients with atrial fibrillation? Results from a multicenter study. *J. Am. Coll. Cardiol.* **2012**, *60*, 531–538. [[CrossRef](#)] [[PubMed](#)]

25. Lee, J.M.; Seo, J.; Uhm, J.S.; Kim, Y.J.; Joung, B. Why Is Left Atrial Appendage Morphology Related to Strokes? An Analysis of the Flow Velocity and Orifice Size of the Left Atrial Appendage. *J. Cardiovasc. Electrophysiol.* **2015**, *26*, 922–927. [[CrossRef](#)] [[PubMed](#)]
26. Bax, J.J.; Marsan, N.A.; Delgado, V. Non-invasive imaging in atrial fibrillation: Focus on prognosis and catheter ablation. *Heart* **2015**, *101*, 94–100. [[CrossRef](#)]
27. Iwasaki, Y.K.; Nishida, K.; Kato, T.; Nattel, S. Atrial fibrillation pathophysiology: Implications for management. *Circulation* **2011**, *124*, 2264–2274. [[CrossRef](#)] [[PubMed](#)]
28. Kreidieh, B.; Rojas, F.; Schurmann, P.; Dave, A.S.; Kashani, A.; Rodríguez-Mañero, M.; Valderrábano, M. Left Atrial Appendage Remodeling After Lariat Left Atrial Appendage Ligation. *Circ. Arrhythmia Electrophysiol.* **2015**, *8*, 1351–1358. [[CrossRef](#)] [[PubMed](#)]
29. Wang, F.; Zhu, M.; Wang, X.; Zhang, W.; Su, Y.; Lu, Y.; Xu, Y. Predictive value of left atrial appendage lobes on left atrial thrombus or spontaneous echo contrast in patients with non-valvular atrial fibrillation. *BMC Cardiovasc. Disord.* **2018**, *18*, 153. [[CrossRef](#)]
30. Olivares, A.L.; Silva, E.; Nuñez-Garcia, M.; Butakoff, C.; Sánchez-Quintana, D.; Freixa, X.; Camara, O. In Silico Analysis of Haemodynamics in Patient-Specific Left Atria with Different Appendage Morphologies. *FIMH* **2017**, *10263*, 412–420. [[CrossRef](#)]
31. Kreidieh, B.; Valderrábano, M. Malignant Left Atrial Appendage Morphology and Embolization Risk in Atrial Fibrillation. *Heart Rhythm Case Rep.* **2015**, *1*, 406–410.



© 2020 by the authors. Licensee MDPI, Basel, Switzerland. This article is an open access article distributed under the terms and conditions of the Creative Commons Attribution (CC BY) license (<http://creativecommons.org/licenses/by/4.0/>).